Journal of Materials Chemistry A

Membrane-controlled CO_2 Electrocatalysts with Switchable C2 Product Selectivity and High Faradaic Efficiency for Ethanol

Journal:	*Journal of Materials Chemistry A*
Manuscript ID	TA-ART-02-2023-000613.R1
Article Type:	Paper
Date Submitted by the Author:	20-Apr-2023
Complete List of Authors:	Akter, Tania; University of Nevada, Reno, Department of Chemistry Barile, Christopher; University of Nevada, Reno, Department of Chemistry

Membrane-controlled CO_2 Electrocatalysts with Switchable C2 Product Selectivity and High Faradaic Efficiency for Ethanol

Tania Akter and Christopher J. Barile*

Department of Chemistry, University of Nevada, Reno, Reno, NV 89557, USA

*E-mail: cbarile@unr.edu

Keywords: CO_2 reduction, electrocatalyst, ethanol, Nafion, proton transport

Abstract

Bimetallic Cu materials are promising CO_2 reduction electrocatalysts for the formation of valuable multicarbon products. We describe membrane-modified Ag-Cu electrocatalysts that convert CO_2 to C2 products with high selectivity. While traditional Ag-Cu catalysts generate ethylene (C_2H_4) as the main product, we demonstrate that product selectivity can be switched to ethanol (C_2H_5OH) by introducing a proton-permeable fluoropolymer. By optimizing the catalyst composition, voltage, and membrane thickness and identity, we develop a catalyst that generates C_2H_5OH with up to 72% Faradaic efficiency, making it the most selective Ag-Cu catalyst for C_2H_5OH reported. Lastly, we discuss a detailed chemical mechanism that explains how the hydrophobicity of the membrane overlayer enables catalysts with switchable C2 product selectivity.

1. Introduction

Electrochemical CO_2 conversion is a promising method of mitigating the greenhouse gas effect and consequent climate change.[1-9] Fuels and chemicals such as methanol, ethanol (C_2H_5OH), ethylene (C_2H_4), ethane, and propanol are attainable value-added CO_2 reduction products.[10-17] Among these products, C_2H_5OH is a useful vehicular fuel that is blended with gasoline at 10 vol. % in the United States and can be used at higher concentrations in flexible-fuel vehicles.[18] In this manner, a carbon neutral emissions cycle is conceivable in which C_2H_5OH is burned to power transportation, and the emitted CO_2 is then electrochemically converted back to C_2H_5OH. C_2H_5OH is also a precursor for the synthesis of various chemical products, and it is used directly in the food and medical industries.[19,20]

Much progress in electrochemical CO_2 reduction has been made since the groundbreaking findings of Hori et al. in the 1980s.[21] Due to the valuable nature of multicarbon products, a large portion of CO_2 reduction research efforts has focused on the development of catalysts that selectively generate C2+ products.[5,12,14,16,22,23] Typically, these catalysts require a high overpotential and must facilitate the generation of catalyst-bound CO intermediates and subsequent dimerization or trimerization to yield the final C2+ products.[14-18,24] Cu-based materials are among the most promising electrocatalysts for the selective generation of C2+ products because they possess an optimal binding energy for surface-bound CO intermediates.[4,10,24-26] However, many Cu-based catalysts still suffer from the slow production rates of C2+ products and low Faradaic efficiencies. Numerous methods have been employed to mitigate these issues including altering catalyst composition,[27] particle size,[28] surface morphology,[27] electrolyte chemistry,[29] and interfacial architecture.[30-32]

In particular, bimetallic Cu catalysts can significantly affect CO_2 reduction product selectivity. Studies from Watanabe et al. showed that different bimetallic compositions including Cu-Ni, Cu-Pb, Cu-Sn, Cu-Zn, Cu-Ag, and Cu-Cd exhibit catalytic behaviors that are distinct from Cu and that in some cases, C2 products are generated.[33,34] Baek et al. demonstrated that a Cu-Zn electrocatalyst produces C_2H_5OH with 25% Faradaic efficiency.[35] Because metal-bound CO is a key intermediate in producing multicarbon products, Ag is an excellent catalyst for CO formation, and Cu facilitates CO-CO coupling, Ag-Cu catalysts are widely employed to generate C2+ products. Among the possible C2+ products, most Ag-Cu catalysts produce C_2H_4 in high yields.[32,36,37]

In this manuscript, we develop Ag-Cu catalysts that selectively produce C_2H_5OH as opposed to C_2H_4 by covering them in proton permeable membranes. Previously, our group demonstrated that membrane-modified CO_2 catalysts can selectively yield CH_4, C_2H_4, or CH_3OH, depending upon the metallic composition of the catalyst and the identity of the membrane.[28,31,32, 38-40] Specifically, a Nafion membrane stabilizes the metal-bound CO intermediate, which enables the formation of highly reduced carbon products. We stress that this means of stabilization using an electrode architecture with a distinct Nafion overlayer is different from simply mixing Nafion with a catalyst to make a composite electrode material in which Nafion functions as a binder.[41] Here, we describe a mechanism that explains how the hydrophobicity of the membrane layer on Ag-Cu catalysts dictates C2 product selectivity and allows for the production of C_2H_5OH with up to 72% Faradaic efficiency.

2. Results and Discussion

2.1. Surface Characterization of Ag-Cu Electrocatalysts modified with Nafion Overlayers

Ag-Cu electrocatalysts were prepared by electrodepositing Cu on Ag surfaces. From the charge passed during the chronoamperometry used for Cu electrodeposition (Figure S1), the average thickness of the Cu is 2.3 μm. An AFM image of the unmodified Ag substrate reveals a relatively smooth morphology with an average roughness of 70 nm (Figure 1A). After Cu electrodeposition, the average roughness increases to 140 nm (Figure 1B). To confirm the thickness of the Cu electrodeposits, we performed AFM across the interface of Ag and Ag-Cu while using the difference in surface roughness to identify the two portions of the electrode (Figure 1C). A height profile across this interface reveals that the thickness of the Cu electrodeposits is about 2 μm (Figure 1D), a value similar to what is calculated from the Cu electrodeposition chronoamperometry.

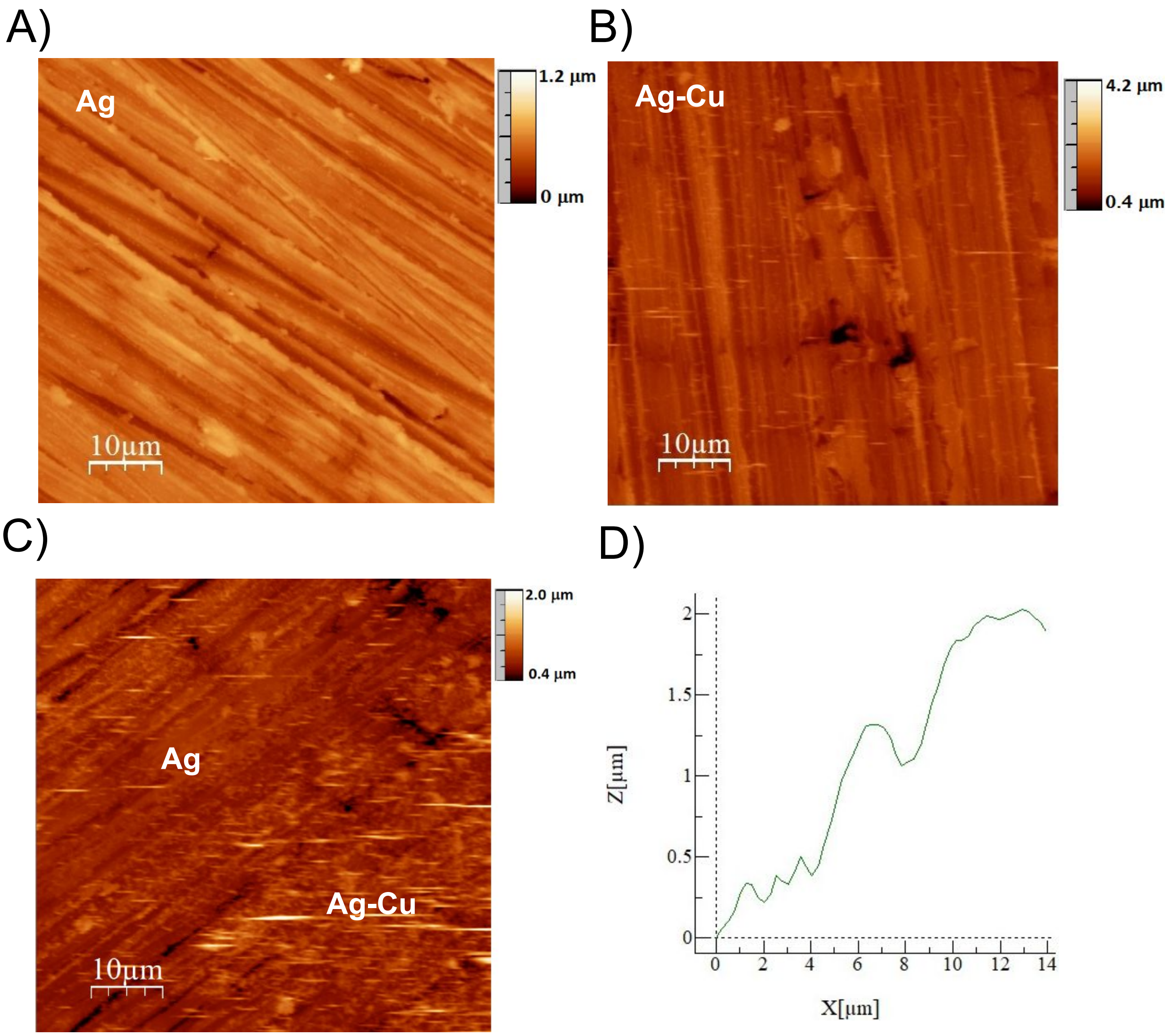

Figure 1. Atomic force microscopy images of unmodified Ag (A), Cu electrodeposited on Ag (Ag-Cu, B), and the interface between unmodified Ag and Ag-Cu (C). A height profile (D) across the interface quantifies the thickness of the electrodeposited Cu.

The Ag-Cu electrodes were then modified with Nafion overlayers of different thicknesses by performing varying rounds of dropcasting. To characterize the surface morphology of the Nafion-modified Ag-Cu electrodes, cross-sectional SEM coupled with energy-dispersive X-ray spectroscopy was conducted (Figure S2). These data, including the F elemental map originating from Nafion, indicate that a relatively uniform layer of Nafion covers the Ag-Cu electrode.

2.2. Linear Sweep Voltammetry of Electrocatalysts

We next conducted linear sweep voltammograms (LSV) of a Ag-Cu electrode and Ag-Cu electrodes modified with Aquivion, Nafion, and PVDF in CO_2-sparged $NaHCO_3$ buffer (Figure 2A). The onset potentials of the LSVs (measured potentials at which 15% of the maximum cathodic current is reached during each voltammogram) of the membrane-modified electrodes are shifted positive compared to unmodified Ag-Cu. This positive shift has been observed previously on membrane-modified Cu, Zn, and brass electrodes[27,38] and is ascribed to changes in proton transfer kinetics, ohmic current, mass transport effects, and the pH of the membrane-electrode interface, all of which impact the LSVs.[27]

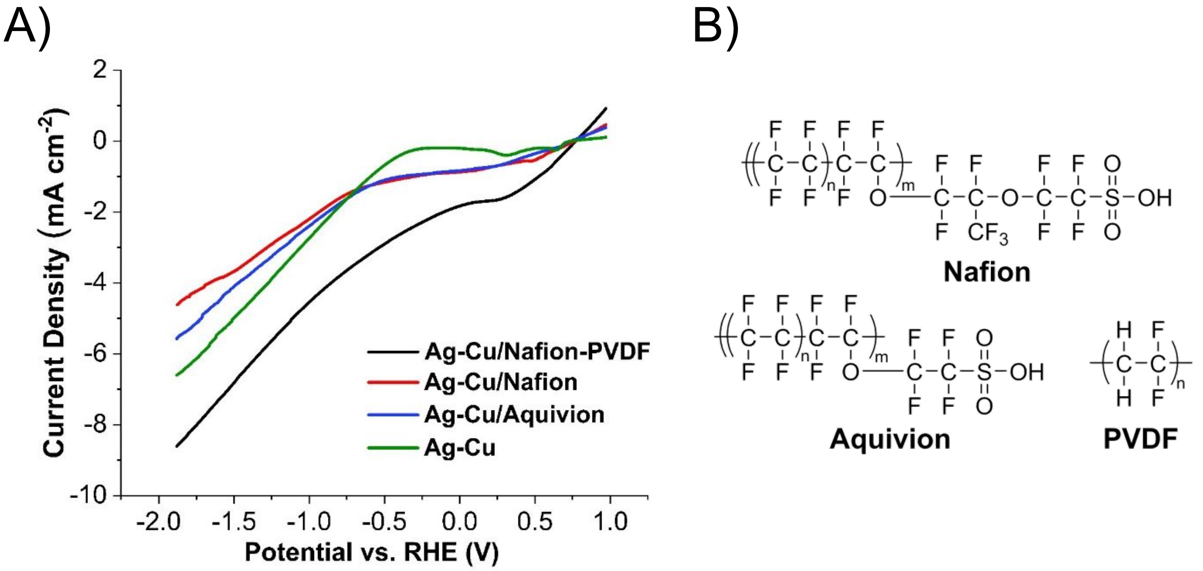

Figure 2. Linear sweep voltammograms (LSVs, A) of Ag-Cu (green), Ag-Cu modified with Aquivion (blue), Ag-Cu modified with Nafion (red), and Ag-Cu modified with 10 wt. % PVDF in Nafion (black) in a CO_2-saturated 0.1 M $NaHCO_3$ electrolyte at a scan rate of 10 mV/s. Structures of the polymers studied (B). The LSVs were obtained after first applying -0.4 V vs. RHE for 1 min to reduce the electrodes.

In particular, unmodified Ag-Cu possesses an onset potential of -0.58 V, whereas the onset potentials for Ag-Cu modified with Aquivion, Nafion, and a composite of Nafion and 10 wt. % PVDF are +0.01 V, +0.26 V, and +0.43 V, respectively. Interestingly, the onset potentials shift to more positive values as the membrane overlayer becomes more hydrophobic. The water contact angles of the electrodes increase in the order of Ag-Cu < Ag-Cu/Aquivion < Ag-

Cu/Nafion < Ag-Cu/Nafion-PVDF, indicating progressively increased hydrophobicity (Figure S3). This trend in hydrophobicity matches chemical intution based upon the structure of the polymers (Figure 2B). Nafion is more hydrophobic than Aquivion because it possesses a longer side chain, which results in a lower density of hydrophillic sulfonate groups.[42] Furthermore, PVDF is the most hydrophobic polymer because it does not possess any sulfonate groups.

The listed onset potentials for the polymer-modified Ag-Cu electrodes described in the above paragraph are more positive than the thermodynamic reduction potentials for CO_2 reduction reactions.[29,36] The onset potentials are reported versus RHE and are calculated using a pH of 6.8, which is the pH of the bicarbonate electrolyte. CO_2 reduction, however, occurs at the polymer-electrode interface, and the interfacial pH is not equal to that of the bulk solution. Aquivion and Nafion are super acids[43,44] with pK_a values of about -6, which indicates that the pH at the interface is significantly lower than 6.8. The result is that the reported onset potentials would be shifted to more negative, thermodynamically acceptable values, according to the Nernst equation.

2.3. CO_2 Reduction Product Distributions

The changes in the onset potentials of the LSVs with different membrane modifications suggest that there might be changes in the distribution of CO_2 reduction products. For the various electrodes, product analyses were conducted after 1 hour of chronoamperometry to elicit CO_2 reduction (Figures S4-S10). Figure 3 exhibits the Faradaic efficiencies (Figure 3A) and rates of formation (Figure 3B) of the CO_2 reduction products from Ag-Cu electrodes modified with 16 μm-thick layers of Nafion, Aquivion, and Nafion-PVDF membranes at -1.9 V vs. RHE. The rates of formation of CO_2 reduction products depend upon the total amount of charge passed in the reactions and the number of electrons transfer per CO_2 reduced. The current densities for the systems evaluated in this manuscript are low compared to several other CO_2 reduction catalysts reported.[45-47] These relatively low current densities are expected because the electrodes used here are fairly flat, unlike highly porous electrodes designed to maximize current density. In future work, we will study nanostructured electrodes and electrodes subjected to flowing electrolyte to maximize current densities.

The distribution of products varies widely as the identity of the membrane on the Ag-Cu electrode is altered. Note that if a product is not listed in Figures 3-6, the product was not detected from the electrode. First, we found that the Ag-Cu electrode produces about 80% C_2H_4 at -1.9 V vs. RHE. Additionally, CH_4, CO, HCOOH, and H_2 are generated as minor products. This finding is consistent with previous studies that demonstrate high C_2H_4 yields with related Ag-Cu systems.[32] The previously reported systems consist of Ag electrodes modified with a composite of Cu nanoparticles dispersed within a Nafion overlayer. The separation of the Ag and Cu active sites of the electrocatalysts results in tandem catalysis that generates C_2H_4. This architecture is different from the Nafion-modified Ag-Cu electrodes described in this work, which do not operate via a tandem pathway and thus enable the formation of other products such as C_2H_5OH. Furthermore, tandem catalysis with Ag and Cu in the absence of a membrane can also result in high yields of CH_4.[48]

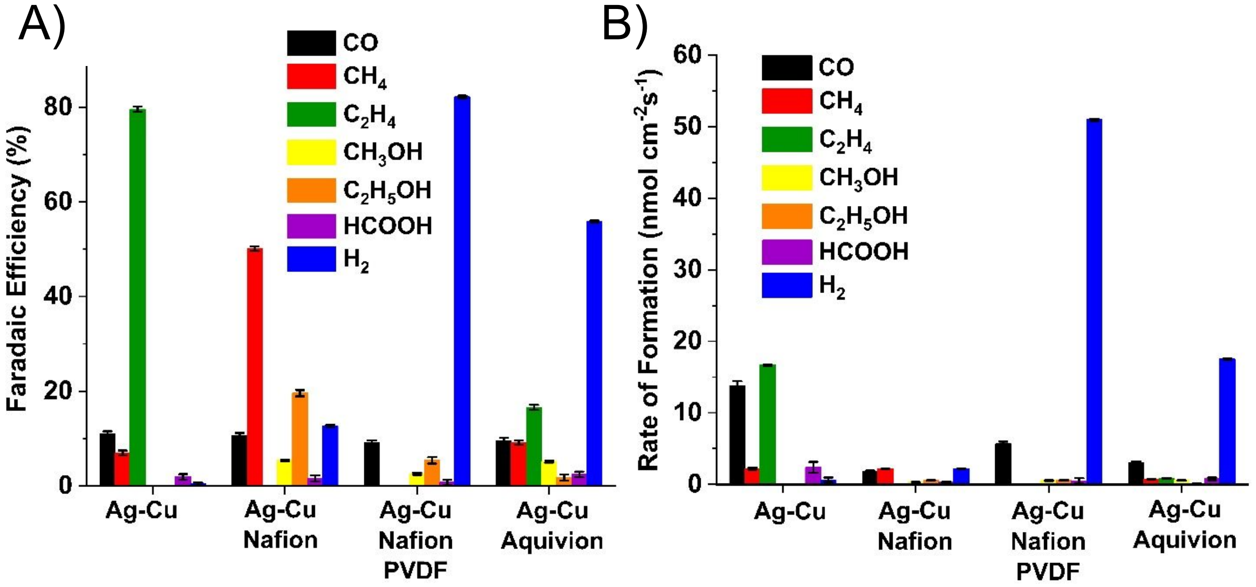

Figure 3. Faradaic efficiencies (A) and rates of formation (B) for CO (black), CH_4 (red), C_2H_4 (green), CH_3OH (yellow), C_2H_5OH (orange), HCOOH (purple), and H_2 (blue) after 1 hr of CO_2 reduction at -1.9 V vs. RHE using Ag-Cu electrodes modified with Nafion, Nafion-PVDF, and Aquivion along with an unmodified Ag-Cu electrode.

Membrane-modified Ag-Cu electrodes show dramatically different product selectivity than unmodified Ag-Cu. For example, Nafion-modified Ag-Cu does not produce any C_2H_4 and instead produces 51% CH_4 and 22% C_2H_5OH. The high yield of CH_4 is attributed to the stabilization of a metal-bound CO intermediate by the Nafion layer, which favors the further reduction of CO to CH_4. The finding that a high yield of CH_4 can be produced with a Nafion-modified electrode matches previous studies with Nafion-modified Cu electrodes.[29] More surprisingly, however, C_2H_5OH is formed without the co-production of C_2H_4, which indicates that the Nafion-modified Ag-Cu electrode yields C_2H_5OH selectively as the only C2 product. Because most previously studied Ag-Cu catalysts do not produce significant quantities of C_2H_5OH and instead generate C_2H_4,[30,49,50] we wondered if we could use this result as a springboard for designing a new class of Ag-Cu catalysts that are selective for C_2H_5OH as the primary product.

To interrogate the parameters that affect C_2H_5OH production, we modified the hydrophobicity of the membrane overlayer. When switching the membrane to a less hydrophobic Aquivion layer, the Faradaic efficiency for C_2H_5OH decreases to 1%, and the C_2H_4 yield increases to 18%. This result indicates that C_2H_5OH vs. C_2H_4 selectivity completely switches when the hydrophobicity of the membrane is decreased. Furthermore, when increasing the membrane hydrophobicity with a Nafion-PVDF layer, the yield of C_2H_5OH decreases to 5% without any C_2H_4 production, and the major product is H_2. Taken together, these results suggest that there is an optimal hydrophobicity of the membrane for the generation of C2 products and C_2H_5OH. We will discuss the mechanistic implications of these findings in the last section of the Results and Discussions portion of this manuscript.

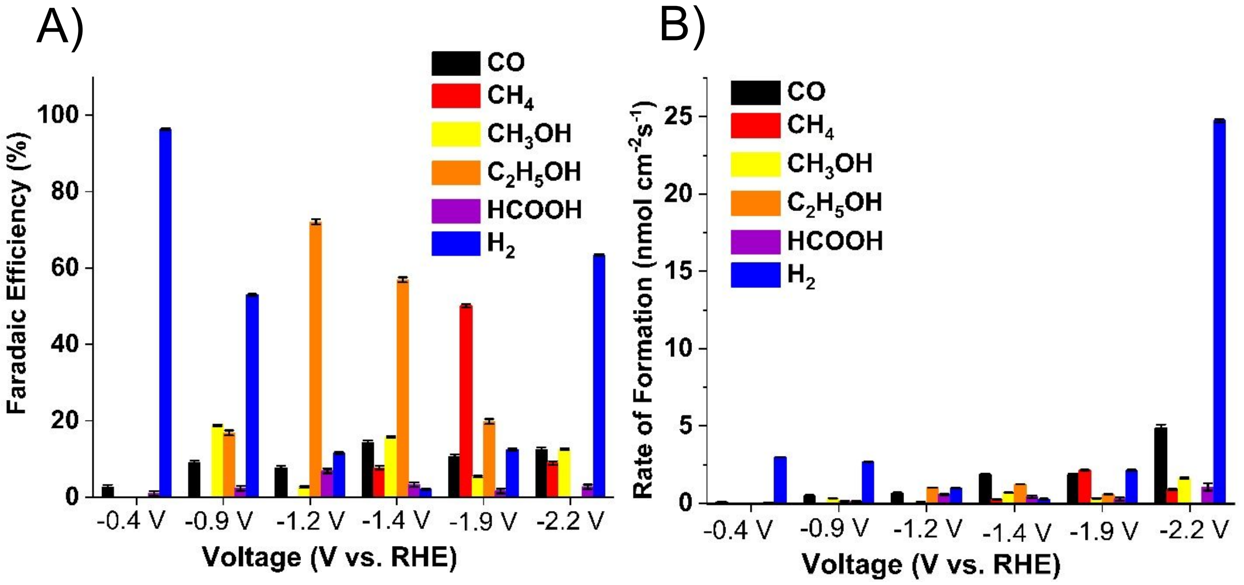

Figure 4. Faradaic efficiencies (A) and rates of formation (B) for CO (black), CH_4 (red), CH_3OH (yellow), C_2H_5OH (orange), HCOOH (purple), and H_2 (blue) after 1 hr of CO_2 reduction at different voltages using Ag-Cu modified with 16 μm of Nafion.

Having established that the Nafion membrane possesses the intermediate hydrophobicity needed to facilitate C_2H_5OH generation, we next varied several electrode attributes of the Nafion-modified Ag-Cu system in an attempt to increase the quantity of C_2H_5OH generated.

First, we evaluated the effect of different CO_2 reduction potentials on product distribution (Figure 4). At -0.4 V vs. RHE, the electrode yields only small percentages of CO and HCOOH along with 98% H_2, indicating that almost no CO_2 reduction happens at this potential. Increasing the potential from -0.4 V to -1.2 V progressively enhances C_2H_5OH production. The overpotential for the production of C_2H_5OH is often higher than those of C1 products due to a rate-limiting C-C coupling step.[51,52] Beyond -1.2 V, the Faradaic efficiency for C_2H_5OH decreases at more negative potentials with CH_4 and H_2 arising as the dominant products at -1.9 V and -2.2 V, respectively. Presumably, at higher overpotentials (-1.9 V), the reduction of CO to CH_4 is kinetically faster than the C-C coupling step needed to generate C_2H_5OH, and at extremely high overpotentials (-2.2 V), H^+ coupling to generate H_2 outcompetes CO_2 chemistry. Regardless, the results demonstrate that -1.2 V is an optimal voltage for C_2H_5OH production, and the 72% C_2H_5OH that is generated at this voltage indicates that the Nafion-modified Ag-Cu electrode is capable of highly selective C_2H_5OH production. The X-ray diffraction (XRD) spectra of the Nafion-modified Ag-Cu electrode before and after electrocatalysis are the same, indicating that the underlining Ag electrode does not undergo significant surface reconstruction during catalysis (Figure S11). The XRD spectra possess peaks corresponding to polycrystalline Ag,[53] but not Cu due to the amorphous nature of the Cu formed by the high electrodeposition voltage (-3 V vs. Ag/AgCl). Furthermore, we also evaluated the longer term ability of the Nafion-modified Ag-Cu electrode to produce high yields of C_2H_5OH. After 10 hours of chronoamperometry at -1.2 V, the electrocatalyst yields C_2H_5OH, CH_3OH, and HCOOH with 70%, 1%, and 7% Faradaic efficiencies, respectively. This result indicates that the catalyst is able to maintain a relatively high selectivity for C_2H_5OH at least over the 10 hours tested.

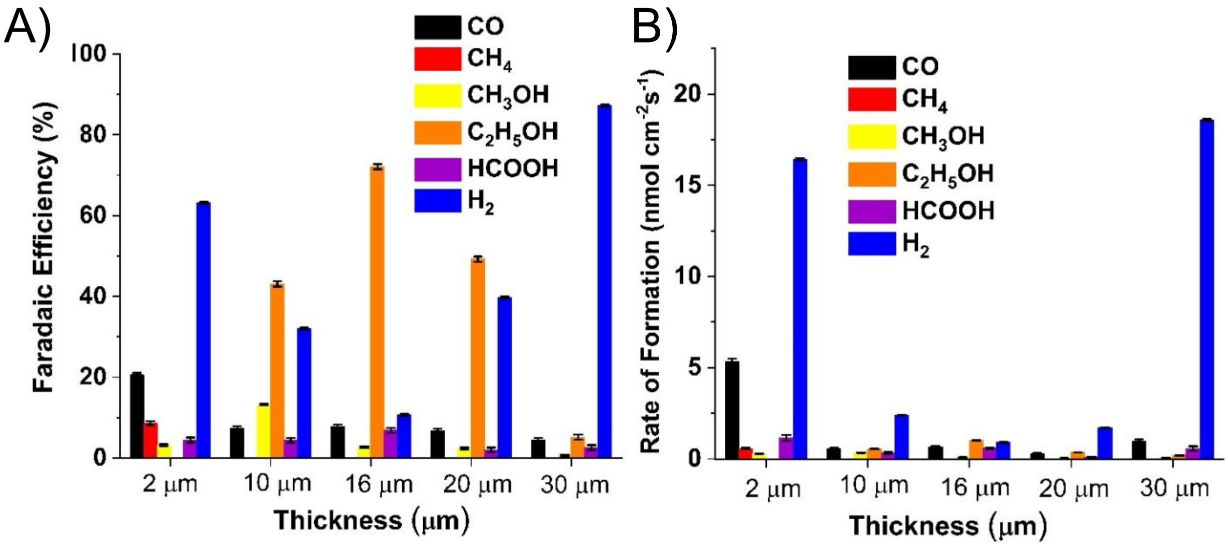

Figure 5. Faradaic efficiencies (A) and rates of formation (B) for CO (black), CH_4 (red), CH_3OH (yellow), C_2H_5OH (orange), HCOOH (purple), and H_2 (blue) after 1 hr of CO_2 reduction at -1.2 V vs. RHE using Ag-Cu modified with various thicknesses of Nafion.

Because the aforementioned experiments utilized 16-μm-thick Nafion, we also analyzed the effect of Nafion thickness on product distribution using -1.2 V vs. RHE, the voltage that is optimal for C_2H_5OH production (Figure 5). With a Nafion layer that is 2 μm thick, the Ag-Cu electrode generates about 62% H_2 and 20% CO as the major products. From 10 μm to 20 μm, significant quantities of C_2H_5OH are generated, and the 72% yield at 16 μm is the highest attained. Further increasing the Nafion thickness to 30 μm results in a substantial decrease in C_2H_5OH yield due to impeded mass transfer of CO_2. H_2 generation predominantly occurs with this thick membrane because it evolves at the Nafion-electrolyte interface as has been explained in analogous cases with thick Nafion layers that impede CO_2 mass transfer.[29] Altogether, these experiments demonstrate that an optimal thickness of the Nafion layer on Ag-Cu is required for tuning mass transport characteristics to produce the highest obtained C_2H_5OH yield of 72%.

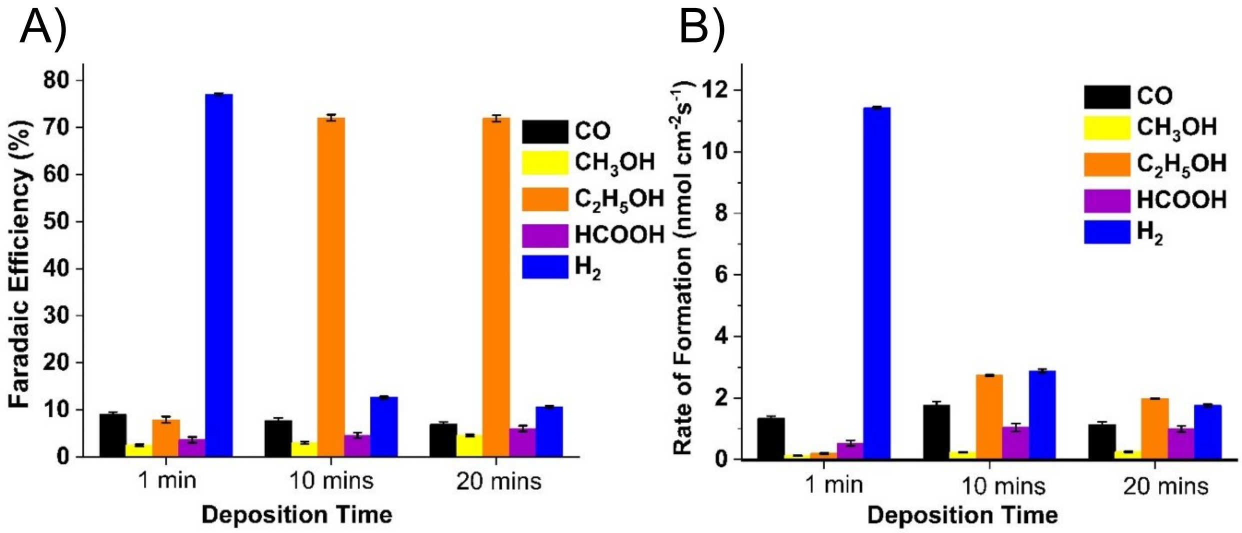

Figure 6. Faradaic efficiencies (A) and rates of formation (B) for CO (black), CH_3OH (yellow), C_2H_5OH (orange), HCOOH (purple), and H_2 (blue) after 1 hr of CO_2 reduction at -1.2 V vs. RHE using Ag-Cu modified with 16 μm of Nafion with varying Cu electrodeposition times.

In addition to varying the membrane thickness in the Nafion-modified Ag-Cu electrode, we also varied the thickness of electrodeposited Cu to evaluate its effect on C_2H_5OH production (Figure 6). It is known that a synergy between Ag and Cu results in the production of C_2H_4.[30] If Cu is electrodeposited for only 1 min, the Cu electrodeposit is visually nonuniform, and the Nafion-modified Ag-Cu electrode yields only small quantities of C_2H_5OH. With 10 min of Cu electrodeposition, however, the Cu conformally covers the Ag surface, and the Nafion-modified electrode generates C_2H_5OH with 72% Faradaic efficiency. An electrode modified with 20 min of Cu electrodeposition results in approximately the same C_2H_5OH yield as the 10 min sample. We expect that a thick enough layer of Cu will prevent the underlining Ag layer from participating synergistically in the electrocatalytic process. However, the amorphous Cu electrodeposits do not adhere well to themselves when they are thick and are partially washed away during electrode fabrication, thus limiting the actual thickness of the Cu electrodeposits to about 2 μm. Even with the nominally 2 μm-thick Cu electrodeposits, the high voltage used during Cu electrodeposition (-3 V vs. Ag/AgCl) results in a heterogeneous and porous Cu layer, thus exposing interfaces between electrolyte, Ag, and Cu on which CO_2 occurs.

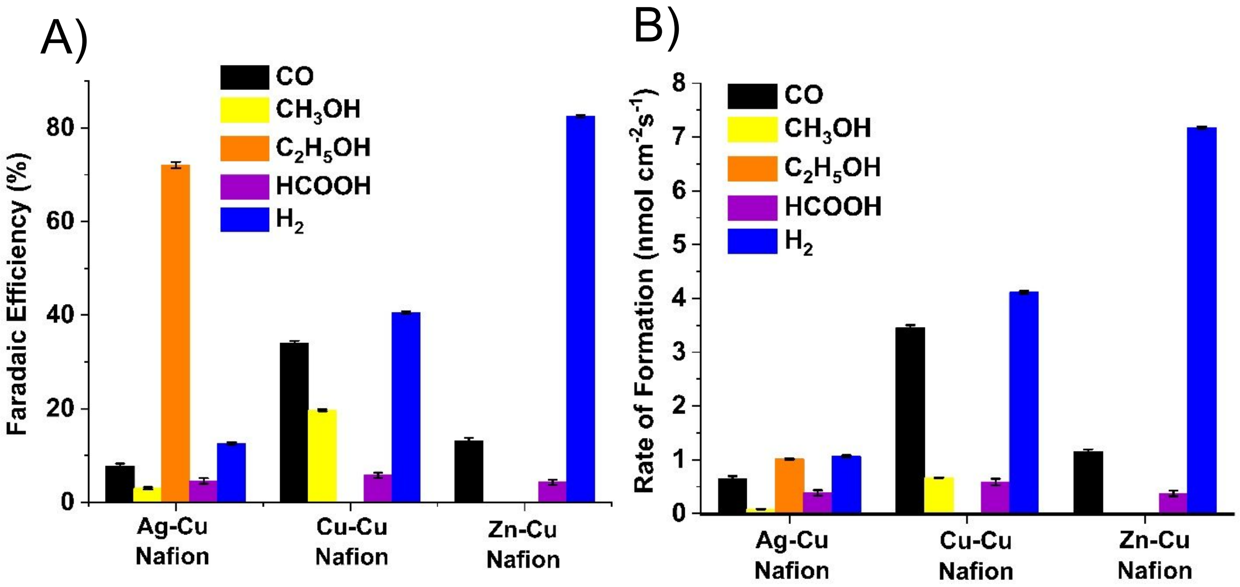

Figure 7. Faradaic efficiencies (A) and rates of formation (B) for CO (black), CH_3OH (yellow), C_2H_5OH (orange), HCOOH (purple), and H_2 (blue) after 1 hr of CO_2 reduction at -1.2 V vs. RHE using Ag-Cu, Cu-Cu, and Zn-Cu modified with 16 μm of Nafion.

To further probe the synergistic role of Ag and Cu, we next tested electrodes with other chemical compositions. In particular, we analyzed the product distributions for Cu and Zn electrodes that are modified with electrodeposited Cu (Figure S12) and subsequently with a 16-μm-thick Nafion membrane (Figure 7). At -1.2 V vs. RHE, the Cu-Cu and Zn-Cu electrodes both with and without Nafion do not generate any C_2H_5OH. These findings indicate that Ag, Cu, and the Nafion membrane must all be present to yield C_2H_5OH.

2.4. Mechanistic Interpretation of Results

The key finding of this manuscript is that the C2 product selectivity for Ag-Cu electrocatalysts can be switched between highly selective (>70% Faradaic efficiency) C_2H_4 and C_2H_5OH production using a membrane architecture. We now rationalize these results in light of previously established mechanisms for these C2 products (Figure 8).[54] The first steps of C_2H_4

and C_2H_5OH formation are the same and result in the formation of a M-O-C_2H_3 intermediate. Ag-Cu catalysts are known to facilitate CO-CO coupling that is needed to generate the M-O-C_2H_3 intermediate. These previously reported Ag-Cu catalysts generally go on to produce C_2H_4 upon further reduction and α-C protonation of the M-O-C_2H_3 intermediate.[54-56] In corroboration of this literature precedent, the Ag-Cu electrocatalyst we fabricate in this work without a membrane also produces a high yield of C_2H_4.

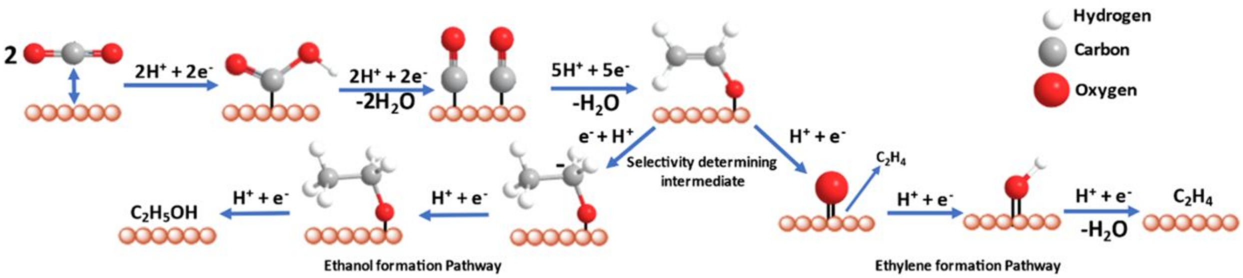

Figure 8. Electrocatalytic CO_2 reduction mechanism for C_2H_5OH and C_2H_4 formation.

To generate C_2H_5OH, β-C protonation of the M-O-C_2H_3 intermediate must occur. In this manner, M-O-C_2H_3 is the selectivity determining intermediate for C_2H_4 vs. C_2H_5OH. We hypothesize that modification of Ag-Cu catalysts with membrane overlayers allows for control over the protonation site (α-C vs. β-C) of this selectivity determining intermediate, which in turn enables a high yield of either C_2H_4 or C_2H_5OH. In particular, it is the degree of membrane hydrophobicity that controls α-C vs. β-C protonation. A relatively hydrophobic membrane is expected to favor β-C protonation and subsequent C_2H_5OH formation because the β-C is in a less polar environment than the α-C since the β-C is further away from the electronegative O atom. The corollary of this interpretation is that a less hydrophobic membrane should favor α-C formation and subsequent C_2H_4 generation.

Indeed, a Ag-Cu electrode modified with Aquivion, a membrane that is less hydrophobic than Nafion, yields C_2H_4 as the predominant C2 product. In contrast, a Ag-Cu electrode modified with a more hydrophobic Nafion membrane produces C_2H_5OH as the only C2 product. A Ag-Cu electrode modified with Nafion-PVDF, which is even more hydrophobic than Nafion, also generates C_2H_5OH as the only C2 product. All three of these experiments are consistent with the above mechanistic interpretations.

Interestingly, the Ag-Cu electrode with Nafion-PVDF yields H_2 with high Faradaic efficiency. This result indicates that the Nafion-PVDF membrane is more hydrophobic than is optimal for CO_2 reduction and that proton transfer to the polymer-electrode interface where CO-CO coupling occurs is significantly impeded. Due to slow proton transfer to the Ag-Cu surface, H_2 is instead produced within the interfaces between the polymer and the electrolyte, interfaces which are not in contact with the Ag-Cu catalyst. This finding is similar to previous studies of PVDF-modified Cu electrodes, which also produce large quantities of H_2.[38] A further experiment performed in D_2O with the Nafion-modified Ag-Cu electrode gives diminished yields of all carbon products (66% C_2H_5OH, 1% CH_3OH, 2% HCOOH, and 4% CO) compared to what the same electrode yields in H_2O. Proton transfer in D_2O is slower than in H_2O,[57] and so D_2 is produced at a higher Faradaic efficiency (27% D_2 vs. 11% H_2), which is consistent with the above mechanistic interpetations.

3. Conclusions

In this manuscript, we design membrane-modified Ag-Cu electrocatalysts for CO_2 reduction with switchable C2 product selectivity. The Ag-Cu catalysts produce C_2H_4 or C_2H_5OH with > 70% Faradaic efficiency. Although a wide variety of Ag-Cu catalysts are known to produce C_2H_4, the 72% Faradaic efficiency for C_2H_5OH reported here is the highest for a Ag-Cu catalyst to the best of our knowledge (Table S1). The observed C2 product selectivities for the various membrane-covered Ag-Cu catalysts are consistent with a detailed mechanistic interpretation that describes control over the protonation site of the key selectivity determining M-O-C_2H_3 intermediate. Taken together, these results provide a new foundation for the rational design of CO_2 reduction electrocatalysts with enhanced selectivity.

4. Experimental Procedures

4.1. Materials and Electrode Preparation

Nafion dispersed in water (10 wt. %) was purchased from Fuel Cell Store (D1021). Aquivion dispersed in water (25 wt. %) was also procured from Fuel Cell Store (D72-25BS) and was diluted with water to 10 wt. % before use. Polyvinylidene fluoride (PVDF) was sold as Kynar Flex 2751-00 and was dispersed in Nafion by sonicating the mixture for 10 min. Ag coins (99.9% purity) were purchased from APMEX, and Cu (99.99% purity) and Zn (99.9% purity) were purchased from Leishent. Ag coins were polished with sandpaper, followed by further polishing with alumina powder (0.05 μm). The Ag was sonicated and rinsed with water before use. Copper (II) sulfate ($CuSO_4$) and sodium bicarbonate ($NaHCO_3$) were purchased from Sigma Aldrich. CO_2 and N_2 gases were purchased from Airgas. Cu was electrodeposited onto the surface of the polished Ag coins in a three-electrode cell using a solution of $CuSO_4$ (50 mM) while performing chronoamperometry at -3.0 V vs. Ag/AgCl for 10 minutes. The electrodes were then gentled washed with water. The Cu/Ag electrodes were then modified with membrane overlayers by drop-casting and letting the dispersion dry under ambient conditions. Multiple rounds of this drop-casting method were used to modulate the thickness of Nafion.

4.2. Materials Characterization

Scanning electron microscopy (SEM) images and energy-dispersive X-ray (EDS) analysis were obtained for each sample using a JEOL JSN-7100F field emission SEM at an acceleration voltage of 15 kV. X-ray diffraction (XRD) measurements were performed using a

Bruker D2 X-ray diffractometer. Atomic force microscopy (AFM) images of the Ag-Cu surface were recorded using a Nanosurf EasyScan 2 microscope operated in contact mode with a silicon tip coated with aluminum (ContAl-G, TedPella, Inc.). A Rame-Hart 100-0 goniometer was utilized to measure water contact angles. Distilled water (40 μL) was dispensed on the dried surfaces, and the angle was measured after 5 s. Reported contact angles for each surface are the average across three droplets.

4.3. Electrochemical Measurements

Electrochemical experiments were performing using a VSP-300 Biologic Potentiostat. All voltage data were measured versus a Ag/AgCl reference electrode and converted to the reversible hydrogen electrode (RHE) scale by V (vs. RHE) = V (measured vs. Ag/AgCl) + 0.21 + 0.059*6.8, where 6.8 is the pH of the CO_2-satured buffer solution. The geometric area of the working electrodes is used for reporting current densities. For linear sweep voltammetry (LSV), the geometric area of the working electrode was 0.22 cm^2, and for chronoamperometry experiments, the geometric area was 5.0 cm^2. To perform electrochemical CO_2 reduction, three-electrode systems (working, reference, and counter electrodes) were studied in 0.1 M $NaHCO_3$ buffer solution sparged with CO_2 gas for at least 15 minutes. Onset potentials were calculated by determining the voltage where current density reached 15% of the maximum current density for each linear sweep voltammogram.

4.4. Product Determination

Electrochemical reduction reactions were performed by applying chronoamperometry to the working electrode for one hour using carbon as a counter electrode in a beaker for ascertaining liquid and solid products and Pt wire as a counter electrode in a custom-designed electrochemical cell for gaseous products (Figure S4). The geometric area of the carbon counter electrode was 19 cm^2 which is substantially greater than the geometric area of the working electrode, which is 5.0 cm^2, so the applied voltage to the counter electrode by the potentiostat is small (<100 mV) during chronoamperometry. This small voltage in the counter electrode does not oxidize any CO_2 reduction products as this is a concern for using an undivided cell. CO_2 was continuously purged at a rate of 5 cm^3/min while performing chronoamperometry in a sodium bicarbonate solution (2.5 mL for gas products and 40 mL for liquid products) at pH 6.8. For gaseous products detection, this flow rate ensures that the products are swept away from the Pt electrode before oxidation occurs. Results using these undivided cells give product distributions for multiple different unmodified polycrystalline metals that are consistent with previous reports with divided cells.[31] Gaseous products were quantified using a SRI 8610C gas chromatograph equipped with a flame ionization detector and a methanizer. Liquid products were analyzed using an Agilent 7890A gas chromatograph coupled to a 5975C quadrupole mass spectrometer (GC-MS). After chronoamperometry, an equal volume of acetonitrile was added to the electrolyte, and the mixture was stored overnight at -15°C. During this process, two separate layers formed, and the top organic layer was separated and dried with anhydrous Na_2SO_4 before conducting GC-MS analysis. The efficiency of this extraction protocol was quantified using standards and accounted for when calculating Faradaic efficiency. For solid product analysis, the bottom aqueous layer was evaporated under reduced pressure, and sodium formate, along with other residues from the electrolyte was dissolved in D_2O for ^1H NMR analysis. ^1H NMR spectroscopy was conducted with a Varian 400 MHz NMR Spectrometer using DMF as an internal standard. In addition to GC-MS methods, ^1H NMR experiments were also conducted to confirm ethanol production. After chronoamperometry, the electrolyte was extracted with $CDCl_3$ (3x 3 mL), and the organic layer was separated and dried with anhydrous Na_2SO_4 before conducting ^1H NMR analysis (Figure S13). Like the GC-MS extraction protocol, the efficiency of the extraction used for ^{1}H NMR analysis was also quantified using standards and accounted for when calculating Faradaic efficiency. All experiments were replicated, and error bars presented are the standard deviation among the multiple trials. The detection limits for the gasses, liquid products, and formate are 1 ppm, 85 μM, and 11 μM, respectively. Faradaic efficiencies were calculated according to the following formula:

$$Faradaic\ efficiency = nFz\ Q * 100\%$$

where n is the number of moles from the generated product, F is Faraday's constant, z is the number of electrons transferred per molecule of the product, and Q is the total charge that is passed during CO_2 reduction.

Author Contributions

All authors designed the experiments, analyzed the data, discussed the results, wrote the manuscript, and commented on the manuscript. T.A. performed the experiments. C.J.B. conceived the project.

Competing Interest

The authors declare no competing interests.

Acknowledgements

This material is based upon work supported by the National Science Foundation CAREER Award under Grant No. CHE-2046105. We acknowledge the Shared Instrumentation Laboratory in the Department of Chemistry at UNR. We gratefully acknowledged the support of National Science Foundation (CHE-1429768) for purchasing X-ray diffractometer. We also acknowledge the Mackay Microbeam Laboratory and Dr. J. DesOrmeau at UNR for assistance with the SEM-EDS analysis.

References

1. T. Takata, J. Jiang, Y. Sakata, M. Nakabayashi, N. Shibata, V. Nandal, K. Seki, T. Hisatomi, K. Domen, *Nature*, **2020,** *581,* 411.
2. R. Shi, Z. Wang, Y. Zhao, G. I. N. Waterhouse, Z. Li, B. Zhang, Z. Sun, C. Xia, H. Wang, T. Zhang, *Nat. Catal.*, **2021,** *4,* 565.
3. J. Zhu, L. Hu, P. Zhao, L. Y. S. Lee, K. Y. Wong, *Chem. Rev.*, **2020,** *120,* 851.
4. D. Karapinar, C. E. Creissen, J. G. Rivera de la Cruz, M. W. Schreiber, M. Fontecave, *ACS Energy Lett.*, **2021,** *6,* 694.
5. H. Xu, D. Rebollar, H. He, L. Chong, Y. Liu, C. Liu, C. J. Sun, T. Li, J. V. Muntean, R. E. Winans, D. J. Liu, T. Xu, *Nat. Energy*, **2020,** *5,* 623.
6. Y. Zhou, F. Che, M. Liu, C. Zou, Z. Liang, P. De Luna, H. Yuan, J. Li, Z. Wang, H. Xie, H. Li, P. Chen, E. Bladt, R. Quintero-Bermudez, T. K. Sham, S. Bals, J. Hofkens, D. Sinton, G. Chen, E. H. Sargent, *Nat. Chem.*, **2018,** *10,* 974.
7. X. Zheng, P. De Luna, F. P. García de Arquer, B. Zhang, N. Becknell, M. B. Ross, Y. Li, M. N. Banis, Y. Li, M. Liu, O. Voznyy, C. T. Dinh, T. Zhuang, P. Stadler, Y. Cui, X. Du, P. Yang, E. H. Sargent, *Joule*, **2017,** *1,* 794.
8. K. P. Kuhl, E. R. Cave, D. N. Abram, T. F. Jaramillo, *Energy Environ. Sci.*, **2012,** *5,* 7050.
9. S. Nitopi, E. Bertheussen, S. B. Scott, X. Liu, A. K. Engstfeld, S. Horch, B. Seger, I. E. L. Stephens, K. Chan, C. Hahn, J. K. Nørskov, T. F. Jaramillo, I. Chorkendorff, *Chem. Rev.*, **2019,** *119,* 7610.
10. X. Su, Z. Jiang, J. Zhou, H. Liu, D. Zhou, H. Shang, X. Ni, Z. Peng, F. Yang, W. Chen, Z. Qi, D. Wang, Y. Wang, *Nat. Commun.*, **2022,** *13,* 1322.
11. D. Yang, Q. Zhu, C. Chen, H. Liu, Z. Liu, Z. Zhao, X. Zhang, S. Liu, B. Han, *Nat. Commun.*, **2019,** *10,* 677.
12. S. A. Francis, J. M. Velazquez, I. M. Ferrer, D. A. Torelli, D. Guevarra, M. T. McDowell, K. Sun, X. Zhou, F. H. Saadi, J. John, M. H. Richter, F. P. Hyler, K. M. Papadantonakis, B. S. Brunschwig, N. S. Lewis, *Chem. Mater.*, **2018,** *30,* 4902.
13. C. S. Chen, J. H. Wan, B. S. Yeo, *J. Phys. Chem. C*, **2015,** *119,* 26875.
14. W. Ma, S. Xie, T. Liu, Q. Fan, J. Ye, F. Sun, Z. Jiang, Q. Zhang, J. Cheng, Y. Wang, *Nat. Catal.*, **2020,** *3,* 478.
15. L. Shang, X. Lv, L. Zhong, S. Li, G. Zheng, *Small Methods*, **2022,** *6,* 2101334.
16. L. Kuo, C.T. Dinh, *Curr. Opin. Electrochem.*, **2021,** *30,* 100807.
17. G. Wu, Y. Song, Q. Zheng, C. Long, T. Fan, Z. Yang, X. Huang, Q. Li, Y. Sun, L. Zuo, S. Lei, Z. Tang, *Adv. Energy Mater.*, **2022,** *12,* 2202054.
18. E. Newes, C. M. Clark, L. Vimmerstedt, S. Peterson, D. Burkholder, D. Korotney, D. Inman, *Energy Policy*, **2022,** *161,* 112713.
19. D. W. Lachenmeier, *J. Occup. Med. Toxicol.*, **2008,** *3,* 26.
20. A. G. Capodaglio, S. Bolognesi, in *Advances in Eco-Fuels for a Sustainable Environment*, ed. K. Azad, Woodhead Publishing, **2019,** pp. 15.
21. Y. Hori, K. Kikuchi, S. Suzuki, *Chem. Lett.*, **1985,** *14,* 1695.
22. G. O. Larrazábal, V. Okatenko, I. Chorkendorff, R. Buonsanti, B. Seger, *ACS Appl. Mater. Inter.*, **2022,** *14,* 7779.
23. E. L. Clark, C. Hahn, T. F. Jaramillo, A. T. Bell, *J. Am. Chem. Soc.*, **2017,** *139,* 15848.
24. Z. Chen, T. Wang, B. Liu, D. Cheng, C. Hu, G. Zhang, W. Zhu, H. Wang, Z. J. Zhao, J. Gong, *J. Am. Chem. Soc.*, **2020,** *142,* 6878.
25. J. Y. Kim, W. Park, C. Choi, G. Kim, K. M. Cho, J. Lim, S. J. Kim, A. Al-Saggaf, I. Gereige, H. Lee, W. B. Jung, Y. Jung, H. T. Jung, *ACS Catal.*, **2021,** *11,* 5658.
26. C. Xiao, J. Zhang, *ACS Nano*, **2021,** *15,* 7975.
27. D. Hursán, A. A. Samu, L. Janovák, K. Artyushkova, T. Asset, P. Atanassov, C. Janáky, *Joule*, **2019,** *3,* 1719.

28. T. Zhang, Y. Qiu, P. Yao, X. Li, H. Zhang, *ACS Sus. Chem. Eng.*, **2019,** *7,* 15190.
29. G. Marcandalli, A. Goyal, M. T. M. Koper, *ACS Catal.*, **2021,** *11,* 4936.
30. L. Ge, H. Rabiee, M. Li, S. Subramanian, Y. Zheng, J. H. Lee, T. Burdyny, H. Wang, *Chem*, **2022,** *8,* 663.
31. H. Pan, C. J. Barile, *Energy Environ. Sci.*, **2020,** *13,* 3567.
32. T. Akter, H. Pan, C. J. Barile, *J. Phys. Chem. C*, **2022,** *126,* 10045.
33. M. Watanabe, M. Shibata, A. Kato, M. Azuma, T. Sakata, *J. Electrochem. Soc.*, **1991,** *138,* 3382.
34. A. Katoh, H. Uchida, M. Shibata, M. Watanabe, *J. Electrochem. Soc.*, **1994,** *141,* 2054.
35. Y. Baek, H. Song, D. Hong, S. Wang, S. Lee, Y. C. Joo, G. D. Lee, J. Oh, *J. Mat. Chem. A*, **2022,** *10,* 9393.
36. J. Wang, Z. Li, C. Dong, Y. Feng, J. Yang, H. Liu, X. Du, *ACS Appl. Mater. Inter.*, **2019,** *11,* 2763.
37. Z. Chang, S. Huo, W. Zhang, J. Fang, H. Wang, *J. Phys. Chem. C*, **2017,** *121,* 11368.
38. H. Pan, C. J. Barile, *ACS Appl. Energy Mater.*, **2022,** *5,* 4712.
39. E. W. Lees, B. A. W. Mowbray, F. G. L. Parlane, C. P. Berlinguette, *Nat. Rev. Mater.*, **2022,** *7,* 55.
40. D. M. Weekes, D. A. Salvatore, A. Reyes, A. Huang, C. P. Berlinguette, *Acc. Chem. Res*, **2018,** *51,* 910.
41. U. O. Nwabara, A. D. Hernandez, D. A. Henckel, X. Chen, E. R. Cofell, M. P. de-Heer, S. Verma, A. A. Gewirth, P. J. A. Kenis, *ACS Appl. Energy Mater.*, **2021,** *4,* 5175.
42. S. H. Shin, P. J. Nur, A. Kodir, D. H. Kwak, H. Lee, D. Shin, B. Bae, *ACS Omega*, **2019,** *4,* 19153.
43. D. J. Jones, in *Polymer Electrolyte Membrane and Direct Methanol Fuel Cell Technology*, eds. C. Hartnig and C. Roth, Woodhead Publishing, **2012,** *vol. 1*, pp. 27.
44. S. Prakash, W. E. Mustain, P. A. Kohl, in *Micro Fuel Cells*, ed. T. S. Zhao, Academic Press, Boston, **2009,** pp. 1.
45. L. X. Liu, Y. Zhou, Y. C. Chang, J. R. Zhang, L. P. Jiang, W. Zhu, Y. Lin, *Nano Energy*, **2020,** *77,* 105296.
46. J. Medina-Ramos, J. L. DiMeglio, J. Rosenthal, *J. Am. Chem. Soc.*, **2014,** *136,* 8361.
47. G. O. Larrazábal, P. Strøm-Hansen, J. P. Heli, K. Zeiter, K. T. Therkildsen, I. Chorkendorff, B. Seger, *ACS Appl. Mater. Inter.*, **2019,** *11,* 41281.
48. H. Zhang, X. Chang, J. G. Chen, W. A. Goddard III, B. Xu, M. Cheng, and Q. Lu, *Nat. Commun.* **2019**, *10*, 3340.
49. C. Chen, Y. Li, S. Yu, S. Louisia, J. Jin, M. Li, M. B. Ross, P. Yang, *Joule*, **2020,** *4,* 1688.
50. D.-L. Meng, M.-D. Zhang, D.-H. Si, M.-J. Mao, Y. Hou, Y. B. Huang, R. Cao, *Ang. Chem. Int. Ed.*, **2021,** *60,* 25485.
51. A. J. Garza, A. T. Bell, M. Head-Gordon, *ACS Catal.*, **2018,** *8,* 1490.
52. Q. Lu, F. Jiao, *Nano Energy*, **2016,** *29,* 439.
53. W. T. Herrera, Y. T. Xing, S. M. Ramos, P. Munayco, M. B. Fontes, E. M. Baggio-Saitovitch, F. J. Litterst, *Phys. Rev. B*, **2011,** *84,* 014430.
54. K. D. Yang, C. W. Lee, K. Jin, S. W. Im, K. T. Nam, *J. Phys. Chem. Lett.*, **2017,** *8,* 538.
55. J. Sans, V. Sanz, P. Turon, C. Alemán, *ChemCatChem*, **2021,** *13,* 5025.
56. C. J. Kong, E. L. Warren, A. L. Greenaway, R. R. Prabhakar, A. C. Tamboli, J. W. Ager, *Sus. Energy Fuels*, **2021,** *5,* 6361-6371.
57. B. J. Siwick, H. J. Bakker, *J. Am. Chem. Soc.*, **2007,** *129*, 13412.